Parametric Study on Taper-ended Tubular Solid Propellant Grains

Mahmoud Y. M. Ahmed
Aerospace Department, Military Technical College, Cairo, Egypt

ABSTRACT

The design of the solid propellant grain is a decisive aspect of the solid propellant rocket motor performance. Tubular grain design is a favorable design since it produces a high neutral (time-invariable) thrust-time profile. However, neutrality of tubular grains deteriorates as the aspect ratio of the grain deviates from an optimum value that is dependent on the web thickness. In some cases, the undesirable phenomenon of erosive grain burning may take place. One simple solution to restore neutrality is to add taper to the ends of the grain. Loss of motor filling comes as penalty for adding these tapered ends. The grain should thus be tailored to simultaneously satisfy both desired design objectives namely, neutrality and filling. The present paper aims to address the dependence of these two design objectives on the design of a taper-ended tubular grain. The designs that are likely to yield erosive burning are also addressed. A parametric study is conducted involving the aspect ratio of the grain, its web thickness, and the taper angles on both ends. These parameters were varied, respectively, in the ranges 0.5: 5, 0.1:0.9, and 10^o:90^o. It was concluded that neutrality and filling of these grains are two competing objectives. The maximum neutrality is achieved using a grain with aspect ratios, web thickness, front and rear taper of 2:2.5, 0.1, 50^o, and 30^o, respectively. In contrast, the maximum filling can be achieved using a grain with aspect ratios and web thickness of 1:3.5 and 0.8, respectively, with no taper at both ends. A compromised grain can have aspect ratio and web thickness of 2 and 0.8, respectively, with no taper at both ends.

Keywords: *Solid propellant rocket propulsion, grain design, neutrality, filling coefficient, erosive burning.*

Nomenclature

A_b	Burning area, [m2]
A_b^*	Burning area-to-grain outer cross section area, [m2]
D_{in}	Inner diameter of propellant grain, [m]

ISSN 1823- 5514, eISSN 2550-164X
Received for review: 2017-04-07
Accepted for publication: 2018-12-26
Published: 2019-04-01

D_{out}	Outer diameter of propellant grain, [m]
K_F	Volumetric filling coefficient, [ ]
L	Length of grain, [m]
L_{out}	Outer length of the grain, [m]
L_{in}	Length of inner cylindrical port of the grain, [m]
L^*	Length- to- diameter ratio , [ ]
y	Instantaneous burnt distance, [m]
θ_h	Head-end taper angle, [deg.]
θ_n	Nozzle-end taper angle, [deg.]
τ	Web thickness, [m]
τ^*	Web thickness-to-grain outer radius ratio, [ ]

Introduction

A rocket motor is an air-independent jet propulsion engine that carries both fuel and oxidizer, the propellant, within itself. Depending on the physical state of the used propellant, rocket motors are classified into rocket motors with solid propellant (SPRM), liquid propellant (LPRM), hybrid propellant (HRM), gel propellant, and cryogenic propellant. Of the two commonly used types, SPRM have many advantages compared with LPRM. Solid propellant rocket motors are simpler in design, easier in maintenance, safer in manipulation, have higher reliability, and longer storage life.
In SPRM, the propellant to be burned is contained within the combustion chamber. The solid propellant charge, the grain, contains all the chemical elements necessary for complete burning. Once ignited, it usually burns smoothly at a predetermined rate on all exposed surfaces of the grain. The internal motor cavity grows as propellant is burned and consumed. the resulting hot gas flows through the supersonic nozzle to impart thrust. Once ignited, the motor combustion proceeds in an orderly manner until essentially all the propellant has been consumed.

Thrust magnitude control is one of potential requirements addressed in some rocket applications. While in LPRM the flow can be modified during flight, it is unmanageable to modify the thrust of SPRM once ignited. To solve this problem in SPRM, tailoring some parameters during the design phase would permit a reasonable predictable thrust history. The desired thrust history (profile) can be achieved via tuning the grain geometry, inhibiting some surfaces, and using different propellant compositions. Generally, the thrust profile of an SPRM can be classified according to its temporal behavior into progressive, regressive, neutral, and dual thrust profiles [1-2]. In neutral profile, the chamber pressure, and hence, the thrust remain approximately constant with time, typically within about +15%. In progressive profile, thrust increases monotonically with time whereas in regressive profile, the thrust decreases monotonically with time. In dual profile, the SPRM yields two

distinct levels of thrust; a high (boost) level followed sharply by a low (sustain) level. Figure 1 compares the possible thrst profiles of solid propellant rocket motors.

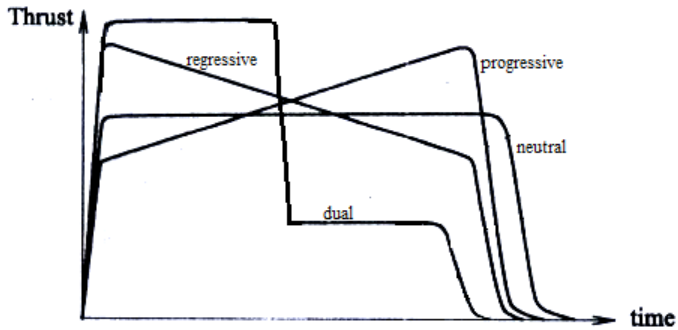

Figure 1: Possible thrst profiles of solid propellant rocket motors

In almost all applications, neutral, single or dual, thrust profiles are desired since they yield the cruise (constant speed) flight preferred for proper flight control especially for guided rockets. A neutral burning is attained using various grain geometries and inhibition styles. The simplest neutral burning grain configuration is the end-burning (cigarette) grain, Fig. 2.a. This configuration also achieves the maximum filling (packing) of the motor cavity. However, the thrust level of the end-burning grains is low due to the small burning area. In contrast, a neutral burning with a high thrust level can be achieved using side (tubular) burning grains, Fig. 2.b. This comes with the penalties of having a short operation time and a low motor filling. The filling of such design can be increased by reducing the inner and outer port areas. However, if the port areas are too small, the gas flow speed along the grain may reach values high enough to cause erosive burning; a phenomenon that produces an undesired progressive burning and yields a large amount of sliver (propellant waste residuals). A compromise between the neutrality and filling can to a great extent be attained using internal burning (perforated) grains, Fig. 2.c. If the perforation along the grain is properly designed, a nearly neutral burning can be achieved. Typical perforation designs are illustrated in Fig. 2.d [1,2]. Clearly, the level of motor packing (filling) varies from one perforation design to another however, the main drawback of such grain design is the complexity of design and production in addition to the possibility of erosive burning in some designs.

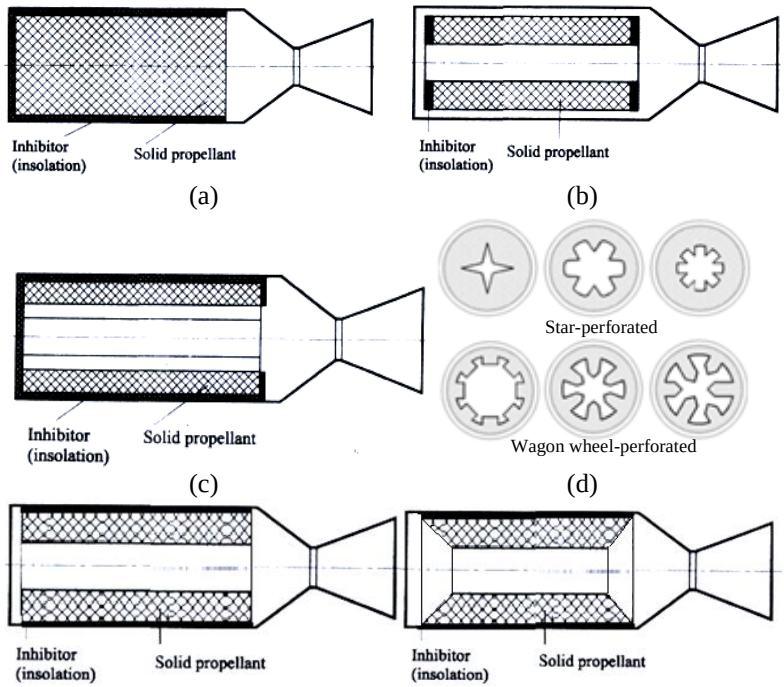

Figure 2: Typical solid propellant grain designs

One simple design that can achieve a neutral burning as well as high motor filling is the end-tubular burning grain. This grain is inhibited from the outer peripheral surface only and is allowed to burn from all other surfaces, Fig. 2.e. If the dimensions of the grain are properly set, a neutral burning can be achieved. Neutrality may deteriorate for longer grains of this type. Adding tapering to grain ends (Fig. 2.f) was found to restore neutrality however, loss in filling emerged as a penalty [3].

Understanding the regression behaviour of solid propellant grains has drawn the efforts of researchers over the years to the extent that recent studies discuss the design optimization of these grains. For instance, design of star perforated grains was discussed by Karman et al. [4], Brooks [5], Krishnan [6] and Albarado et al. [7]. The designs of finocyl grains, tubular grains with radial slots, and wagon-wheel grains were examined by Nisar et al. [8], Kamran and Guozhu [9], and Raza and Liang [10-12], respectively.

Desipte its design simplicity compated with perforated grains, taper-ended tubular grains have drawn the least attention of researchers. Since their introduction as a patent in 1961 by Kirchner [13], almost no work was reported on these grains in the open literature. Shekhar [14] examined the neutrality of

tubular grains with one tapered end. He developed mathematical expressions for the area of the burning surface and investigated the effects of varying the grain length, web thickness, and taper angle. Noaman et al. [3] examined neutrality and filling of the tubular grain tapered at both ends for web thickness of 0.4 and three values of taper angles (equal in both sides).

Neutrality and filling of these taper-ended tubular grains are believed to be dependent on the their configuration. The present work is intended to conduct a parametric study on the dependence of neutrality and filling of such grains on their design. Mathematical expressions for these two merits are derived in terms of the grain design parameters and are applied for a large number of distinct designs that are generated using a space-filling sampling approach. The present work can be viewed as an extension for the work of Noaman et al. [3] with web thickness varied, unequal taper angles on both ends, and the entire design space is expanded. In addition, along with neutrality and filling, erosive burning that may take place for some designs is taken into consideration. This likelihood is addressed for specific ballistic environment. The maximum combustion gas flow velocity along the grain is taken as a measure of erosive burning occurrence. The remainder of the paper is organized as follows. The sampling methodology is presented next along with the full derivations for neutrality, filling, and erosive burning measure. The following section presents and discusses the main findings of the study. The paper finalizes with main conclusions of the study.

Case study and Methodology

Case study and sampling approach

The geometry of the taper-ended tubular grain in concern is shown in Fig. 3. For a given rocket motor caliber, D_{out}, the grain geometry can be fully represented by four independent geometrical parameters namely, the web thickness, the grain length, and the taper angles on both sides of the grain. For a more generic representation, the web thickness and grain length are referred to the grain caliber, D_{out}, as follows:

The relative web thickness:

$$\tau^* = \frac{2\tau}{D_{out}} = 2 * \frac{0.5 * (D_{out} - D_{in})}{D_{out}} = 1 - \frac{D_{in}}{D_{out}}$$

The mean grain slenderness ratio:

$$L^* = \frac{L}{D_{out}} = 0.5 * \frac{(L_{out} + L_{in})}{D_{out}}$$

The head-end taper angle: θ_h

The nozzle-end taper angle: θ_n

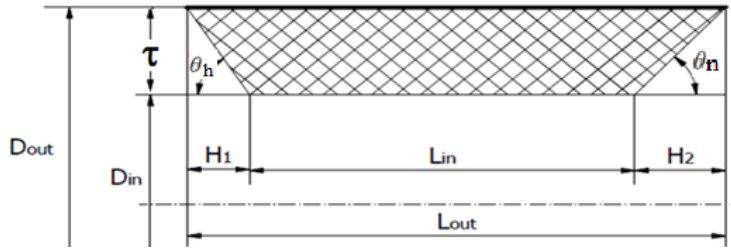

Figure 3: Configuration and design parameters of taper-ended tubular grains

By independently varying these four parameters within some upper and lower respective bounds, various distinct designs can be generated. In this work, the lower and upper bounds of variation for these four parameters are listed in Table 1.

Table 1: Lower and upper bounds of grain design parameters

Design parameter	Lower bound	Upper bound
Relative web thickness, τ^*	0.1	0.9
Mean grain slenderness ratio, L^*	0.5	5
Head-end taper angle, θ_h	10^o	90^o
Nozzle-end taper angle, θ_n	10^o	90^o

Samples are selected from the developed four-dimensional design space using the full-factorial sampling technique. With 9, 10, 9 and 9 divisions for τ^*, L^*, θ_h, and θ_n, respectively, a total of 7290 samples (each representing a distinct grain design) is generated. For each design, the neutrality, filling, and erosive burning criterion is calculated using the formula derived below.

Neutrality Coefficient

Neutrality of burning is express how the produced thrust maintains a constant value over the motor operation time. For solid propellant grains, neutrality is achieved if the area of burning surface maintains a nearly constant value over the entire operation time. There are many measures of neutrality; here, the ratio between the maximum and average burning surface areas of the grain is taken as a measure of neutrality. Following this definition, neutrality coefficient is generally greater than 1 and the best neutrality value is 1 which indicates that the maximum burning surface area is equal to the average burning surface area. In what follows, this expression for neutrality is derived under the following two assumptions:

During the burning process, the burning surface moves parallel to the initial surface, Fig. 4. At any instant of time, the dashed line marks the instantaneous burning surface.

The length of the inner cylindrical port, L_{in}, remains greater than zero over the entire motor operation time. Hence, an axial section along the burning surface

will retain a trapezoidal rather than a triangular shape over the entire burning time. This implies that the grain dimensions are such that it is consumed axially from both sides before the inner cylindrical surface reaches the outer one. Out of the 7290 samples generated in the design space presented above, 551 samples violate this condition and are eliminated from the samples.

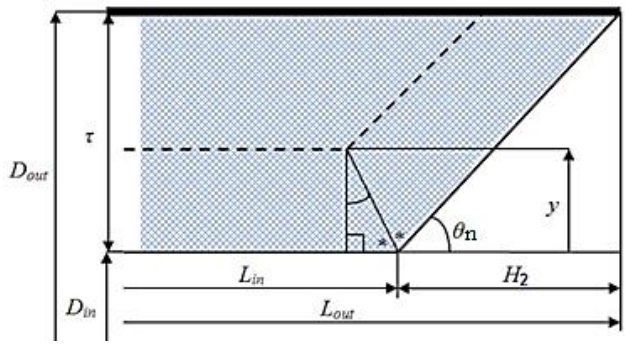

Figure 4: Regression style of the grain

Following the above assumptions, for a given burnt distance, y, the burning area can be expressed as:

$$A_b = \pi(D_{in} + 2y)\left[L_{in} - y\left(\tan\left(\frac{\theta_h}{2}\right) + \tan\left(\frac{\theta_n}{2}\right)\right)\right] + \frac{\pi}{2}(D_{out} + D_{in} + 2y)\left[\left(\frac{\tau - y}{\sin(\theta_h)}\right) + \left(\frac{\tau - y}{\sin(\theta_n)}\right)\right] \quad (1)$$

Substituting in the above equation for the following geometric relations:

$L_{in} = L - \frac{H_1}{2} - \frac{H_2}{2}$,

(H_1 and H_2 are the front and rear taper lengths; shown in Fig. 3)

$$\tan\left(\frac{\theta}{2}\right) = \frac{1}{\sin(\theta)} - \frac{1}{\tan(\theta)}$$

$$H_1 = \frac{\tau}{\tan(\theta_h)} \qquad H_2 = \frac{\tau}{\tan(\theta_n)}$$

$$D_{in} = D_{out} - 2\tau$$

Equation (1) will have the form:

$$A_b = \pi \left[L(D-2\tau) - \frac{2yD}{\sin(\theta_h)} - \frac{2yD}{\sin(\theta_n)} + \frac{3y\tau}{\sin(\theta_h)} + \frac{3y\tau}{\sin(\theta_n)} + \frac{yD}{\tan(\theta_h)} + \frac{yD}{\tan(\theta_n)} - \frac{3y\tau}{\tan(\theta_h)} - \frac{3y\tau}{\tan(\theta_n)} + 2yL - \frac{3y^2}{\sin(\theta_h)} - \frac{3y^2}{\sin(\theta_n)} + \frac{2y^2}{\tan(\theta_h)} + \frac{2y^2}{\tan(\theta_n)} - \frac{\tau D}{2\tan(\theta_h)} - \frac{\tau D}{2\tan(\theta_n)} + \frac{\tau^2}{\tan(\theta_h)} + \frac{\tau^2}{\tan(\theta_n)} + \frac{\tau D}{\sin(\theta_h)} - \frac{\tau^2}{\sin(\theta_h)} - \frac{\tau^2}{\sin(\theta_n)} + \frac{\tau y}{\sin(\theta_h)} + \frac{\tau y}{\sin(\theta_n)} \right] \quad (2)$$

Now, introducing the following dimensionless terms:

$$A_b^* = \frac{A_b}{\frac{\pi}{4} D_{out}^{\ 2}} \qquad \tau^* = \frac{2\tau}{D_{out}} \qquad y^* = \frac{y}{\tau} \qquad L^* = \frac{L}{D_{out}}$$

Eventually, Eqn. (2) will have the form:

$$A_b^* = a + by^* + cy^{*2}$$

where:

$$a = 4L^* - 4\tau^* L^* - \frac{\tau^*}{\tan(\theta_h)} - \frac{\tau^*}{\tan(\theta_n)} + \frac{\tau^{*2}}{\tan(\theta_h)} + \frac{\tau^{*2}}{\tan(\theta_n)} + \frac{2\tau^*}{\sin(\theta_h)} + \frac{2\tau^*}{\sin(\theta_n)} - \frac{\tau^{*2}}{\sin(\theta_h)} - \frac{\tau^{*2}}{\sin(\theta_n)}$$

$$b = -\frac{4\tau^*}{\sin(\theta_h)} - \frac{4\tau^*}{\sin(\theta_n)} + \frac{4\tau^{*2}}{\sin(\theta_h)} + \frac{4\tau^{*2}}{\sin(\theta_n)} + \frac{2\tau^*}{\tan(\theta_h)} + \frac{2\tau^*}{\tan(\theta_n)} - \frac{3\tau^{*2}}{\tan(\theta_h)} - \frac{3\tau^{*2}}{\tan(\theta_n)} + 4\tau^* L^*$$

$$c = -\frac{3\tau^{*2}}{\sin(\theta_h)} - \frac{3\tau^{*2}}{\sin(\theta_n)} + \frac{2\tau^{*2}}{\tan(\theta_h)} + \frac{2\tau^{*2}}{\tan(\theta_n)}$$

Finally, neutrality is defined as the ratio of the maximum to the average burning surfaces encountered during the burning duration, i.e.,:

$$N = (A_b^*)_{max} / (A_b^*)_{average} \quad (4)$$

where:

$$(A_b^*)_{max} = a - \frac{b^2}{4c} \qquad (A_b^*)_{average} = a + \frac{b}{2} + \frac{c}{3}$$

Filling Coefficient

The filling reflects the level of packing of propellant inside the rocket motor. Here, the coefficient of volumetric filling is implemented to describe the level of filling. It is defined as the ratio of the grain volume to the available empty motor volume. These two volumes are expressed, respectively, as:

$$V_P = \frac{\pi}{4}(D_{out}^2 - D_{in}^2)L = \frac{\pi}{4}[D_{out}^2 - (D_{out} - 2\tau)^2]L = \frac{\pi}{4}L(4D_{out}\tau - 4\tau^2)$$

$$V_m = \frac{\pi}{4}L_{out}{D_{out}}^2 = \frac{\pi}{4}\left(L + \frac{H_1}{2} + \frac{H_2}{2}\right){D_{out}}^2 = \frac{\pi}{4}\left[L + \frac{\tau}{2\tan(\theta_h)} + \frac{\tau}{2\tan(\theta_n)}\right]{D_{out}}^2$$

Hence, the volumetric filling coefficient is expressed as:

$$K_F = \frac{V_P}{V_m} = \left[\frac{1}{1 + \left(\frac{\tau}{2L}\right)\left(\frac{1}{\tan(\theta_h)} + \frac{1}{\tan(\theta_n)}\right)}\right]\left[\frac{4\tau D_{out} - 4\tau^2}{{D_{out}}^2}\right] = (2\tau^* - \tau^{*2})\left[\frac{1}{1 + \left(\frac{\tau^*}{4L^*}\right)\left(\frac{1}{\tan(\theta_h)} + \frac{1}{\tan(\theta_n)}\right)}\right] \quad (5)$$

The volumetric filling coefficient has a theoretical maximum value of 1; a value of this coefficient closer to 1 is better.

Erosive burning

Erosive burning is defined as the augmentation of grain burning rate due to excessive gas flow speed along the grain port [1, 2]. Clearly, erosive burning is undesirable since it yields unpredictable thrust profiles as well as considerable amount of sliver. As a rule of thumb, if the velocity of combustion gases through the port reaches 200 m/s, erosive burning occurs. For the grain configuration considered in this study, erosive burning can take place in some designs and it is desired to determine these designs. To do so, the maximum combustion gas velocity is estimated. It is the gas velocity at the nozzle-end of inner cylindrical port of the grain immediately at the onset of combustion calculated as:

$$A_P = \frac{\pi}{4}{D_{in}}^2 = \frac{\pi}{4}(D_{out} - 2\tau)^2$$

The gases flowing through this area are generated as a result of combustion of all upstream burning surfaces calculated as:

$$A_g = \pi D_{in} L_{in} + \frac{\pi}{2}(D_{in} + D_{out})\left[\frac{\tau}{\sin(\theta_h)}\right]$$
$$= \pi(D_{out} - 2\tau)\left(L - \frac{\tau}{\tan(\theta_h)} - \frac{\tau}{\tan(\theta_n)}\right)$$
$$+ \frac{\pi}{2}(2D_{out} - 2\tau)\left[\frac{\tau}{\sin(\theta_h)}\right]$$

Dividing A_g by A_P,

$$\frac{A_g}{A_P} = \frac{4\left(L - \frac{1}{2}\left(\frac{\tau}{\tan(\theta_h)} + \frac{\tau}{\tan(\theta_n)}\right)\right)}{D_{out} - 2\tau} + \left(1 + \frac{D_{out}}{D_{out} - 2\tau}\right)\left(\frac{\tau}{(D_{out} - 2)\sin(\theta_h)}\right)$$

Dividing both nominator and denominator by $\frac{\pi}{4}{D_{out}}^2$,

$$\frac{A_g}{A_P} = \frac{4}{(1-\tau^*)}\left[L^* - \frac{1}{2}\left(\frac{\tau^*}{\tan(\theta_h)} + \frac{\tau^*}{\tan(\theta_n)}\right)\right] + \left(1 + \frac{1}{1-\tau^*}\right)\left[\frac{\tau^*}{(1-\tau^*)\sin(\theta_h)}\right] \quad (6)$$

Based on continuity principle, the mass flow rate of combustion gases through any given port is equal to their rate of generation from all upstream surfaces [3]. Hence:

$$V_g A_P \rho_g = A_g \rho_{sp} r \qquad \text{or:} \qquad V_g = \frac{A_g}{A_P}\frac{\rho_{sp}}{\rho_g} r$$

where A_g/A_P is defined in Eqn. (6) and ρ_{sp} and ρ_g are the densities of the solid propellant and combustion gas products, respectively. r is the rate of burning of the propellant that is dependent on the combustion pressure through the burning law relation [1, 2]. For any design, if V_g exceeds the value of $200\ m/s$, erosive burning takes place causing the undesirable excessive regression pattern. Clearly, estimating the erosive burning requires specifying the ballistic properties of the used propellant. Here, the properties of a typical double-base propellant listed in the table below are used.

Table 2: Ballistic properties of the used propellant for erosive burning calculations

Ballistic property	Value
Combustion pressure, P_c [bar]	70
Burning law	$r = 0.713 \times 10^{-5} P^{0.569}$
Burning rate at P_c, [m/s]	0.008
Propellant density, ρ_{sp}, [Kg/m^3]	1563
Combustion gas density, ρ_g, [Kg/m^3]	6.05

Results and Discussions

Samples distribution in the objective space

Figure 5a below shows the distribution of all samples in the two-dimensional objective space with neutrality and filling as the space coordinates. Here, only the 6738 samples that obey the constraints for inner cylinder length are plotted. The solid markers refer to the samples that encounter erosive burning based on the ballistic conditions proposed in the previous section. The hollow markers refer to the samples that are expected to experience no erosive burning. A zoom-in at the Pareto front (the set of competing designs) of all samples is illustrated in Fig. 5b whereas Fig. 5c shows the Pareto front of all samples with no erosive burning.

It is clear that the two objectives namely, maximum filling and minimum neutrality are competing. A single sample that possesses both maximum filling and minimum (best) neutrality does not exist. As the filling coefficient values of the samples approach the maximum value of 1, the corresponding neutrality coefficient values shift further higher than the minimum value of 1. In addition, samples that have the upper values of filling; samples with filling higher than 0.96 always encounter erosive burning.

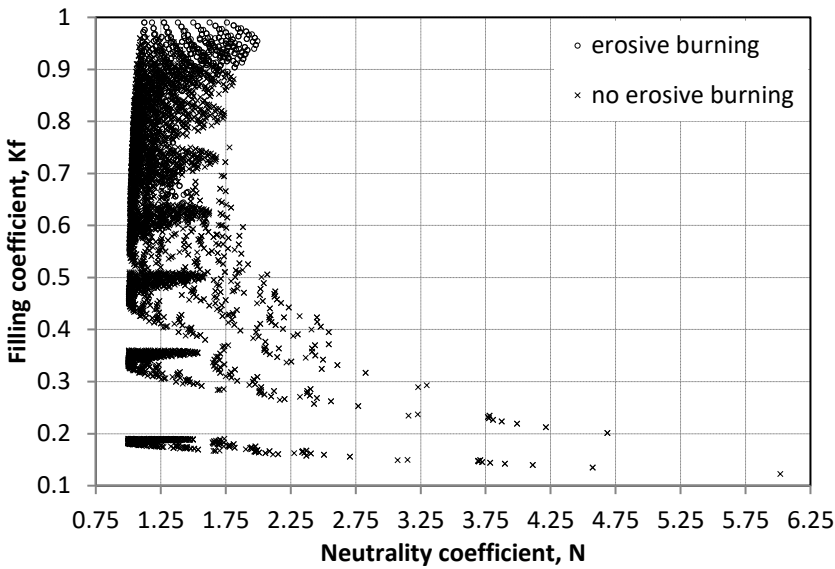

(a)

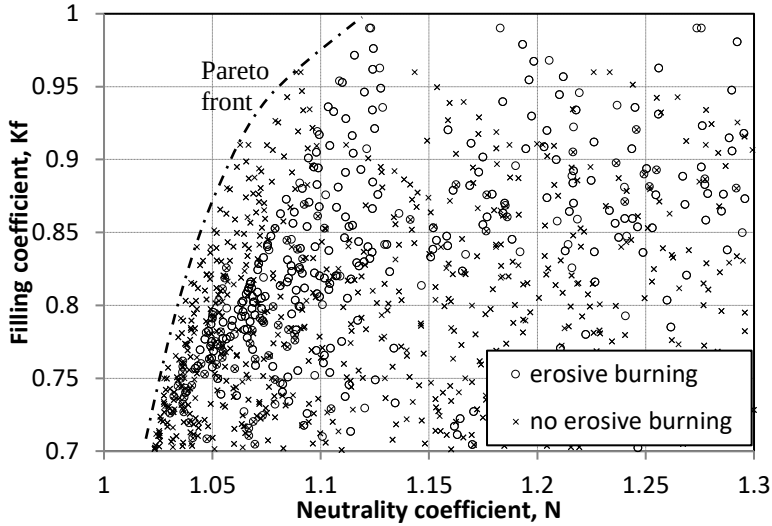

(b)

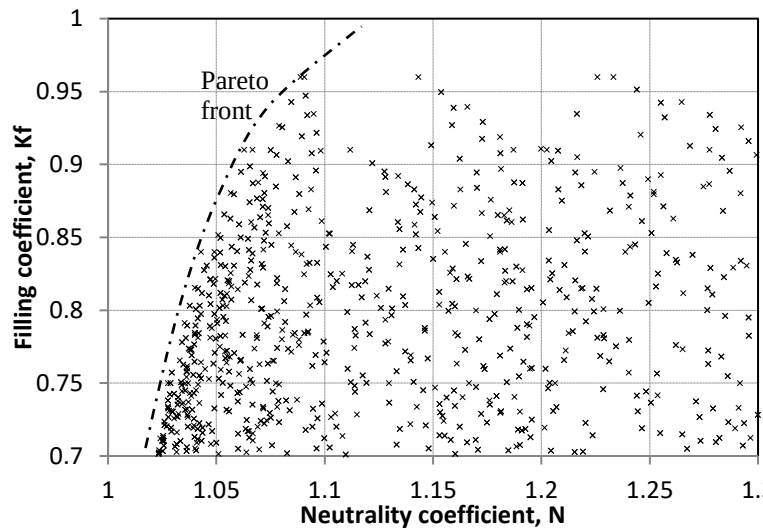

(c)

Figure 5: Distribution of samples in the objective space

Variation of filling coefficient with the design parameters

Figure 6 illustrates samples of the variation of filling coefficient with the grain design parameters. Examining the above figures reveals the following. Grain filling coefficient increases with the increase in web thickness for all grain lengths. For a given web thickness, as the taper angles on both ends increases, the filling increases; perfectly cylindrical grains (with no taper ends) yield the

maximum filling. The effect of taper angles is insignificant in grains with small web thickness and becomes more pronounced as the web thickness increases. The impact of grain length on filling coefficient may not be clear in the above figure. This role is illustrated more clearly in Fig. 7 below.

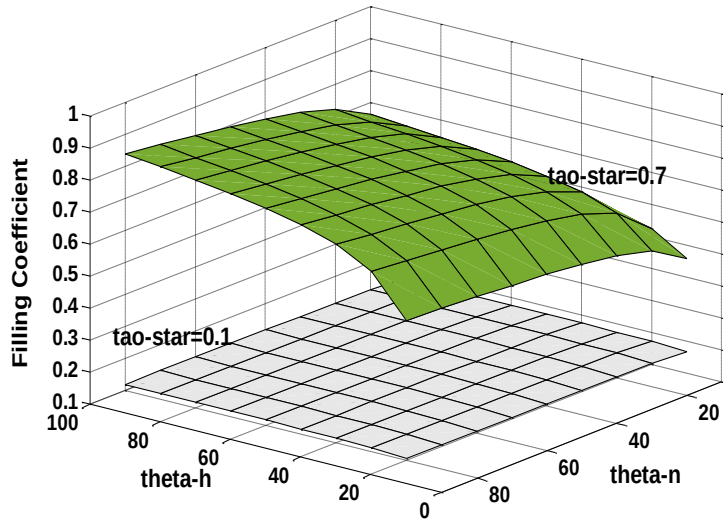

(a) $L^* = 2$

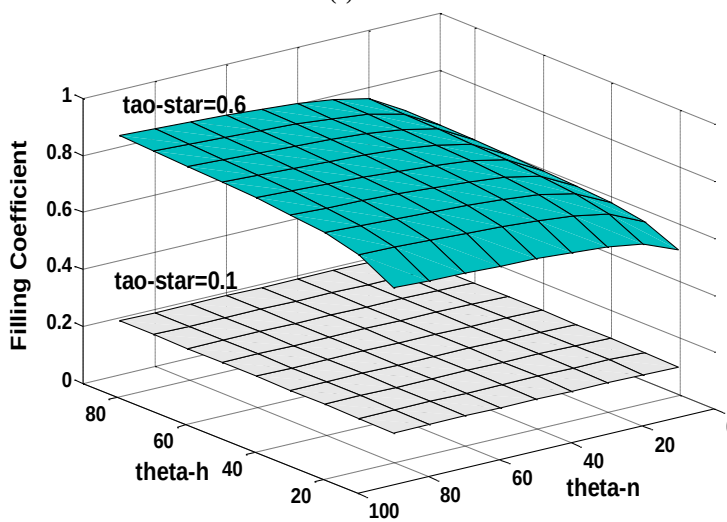

(b) $L^* = 4$

Figure 6: Variation of filling coefficient with design parameters for (a) $L^* = 2$ and (b) $L^* = 4$

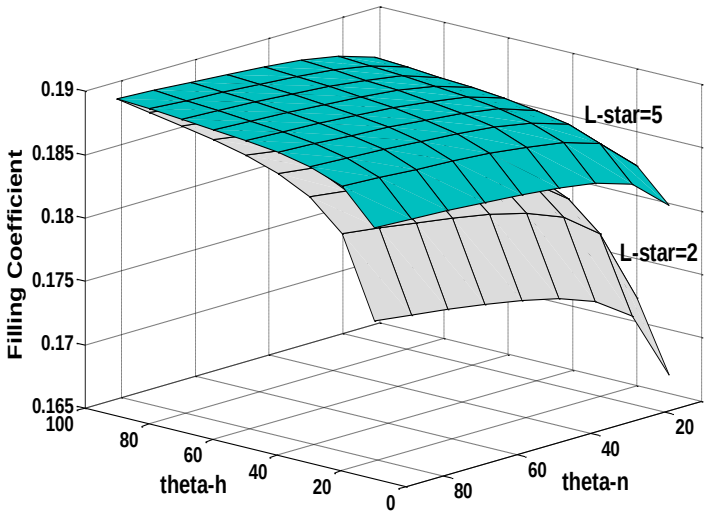

(a) $\tau^* = 0.1$

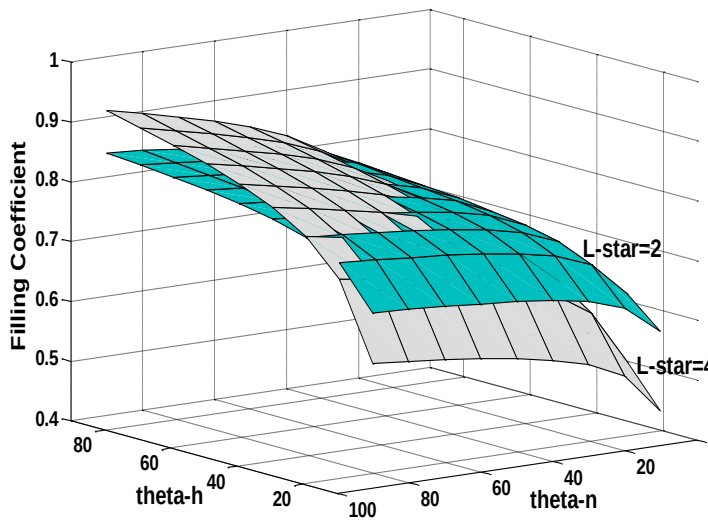

(b) $\tau^* = 0.6$

Figure 7: Variation of filling coefficient with design parameters for (a) $\tau^* = 0.1$ and (b) $\tau^* = 0.6$

As inferred from Figures 6 and 7, for grains with small web thickness, as the grain length increases, the filling improves however, this role is more pronounced at small taper angles. For perfectly cylindrical grains (with small web thickness), the grain length has an insignificant effect on the filling coefficient. In contrast, for grains with large web thickness and small taper angles, shorter grains yield higher filling than longer ones. On the other hand,

a higher filling can be achieved with large web thickness and high taper angles if longer grains are used.

Variation of neutrality with the design parameters:

Figure 8 illustrates samples of the variation of neutrality coefficient with the design parameters.

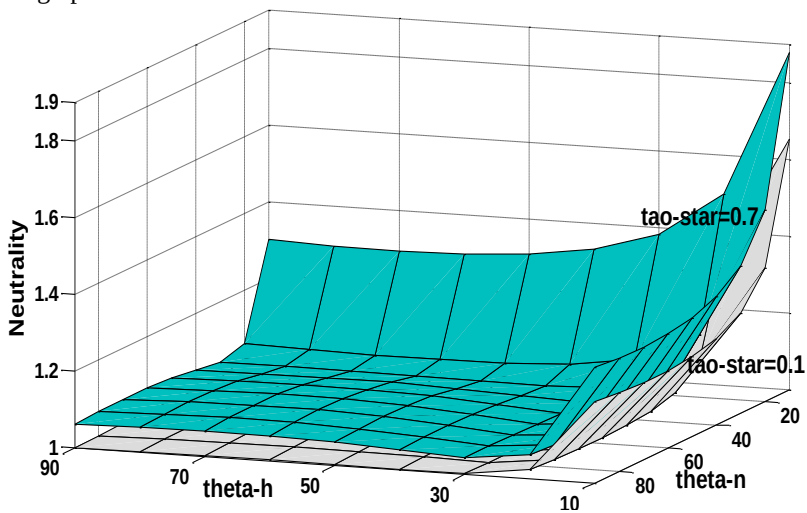

Figure 8: Variation of neutrality coefficient with design parameters for $L^* = 2$

Figure 8 shows that neutrality increases as the web thickness increases for all grain lengths. For short grains, the best (minimum) neutrality is achieved at high taper angles and becomes higher (worse) as the taper angles decrease. For longer grains, the behavior of neutrality changes. The best (minimum) neutrality is associated with small taper angles. It then deteriorates (increases) as the taper angles increase (up to about 60^o) and slightly improves as the taper angles increase further. The dependence of neutrality coefficient can be further understood from Fig. 9.

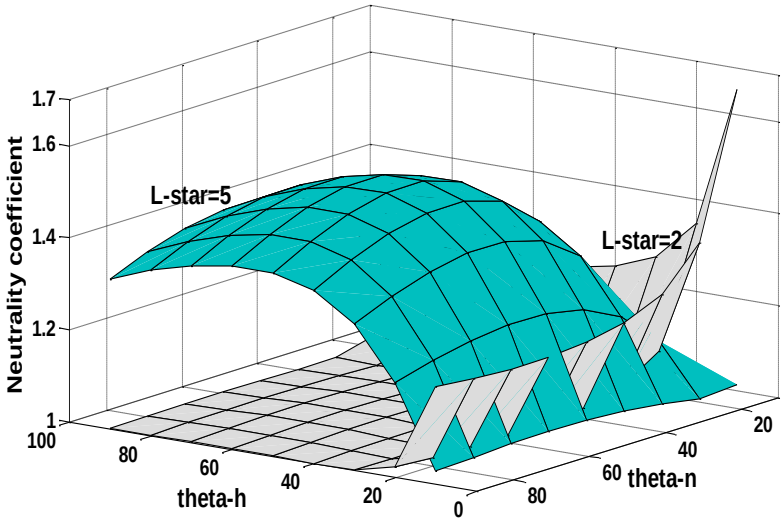

Figure 9: Variation of neutrality coefficient with design parameters for $\tau^* = 0.1$

Design parameters of extreme and compromised grain designs:

Finally, the design parameters of grains that show the extreme (maximum and minimum) values of both merits namely, filling and neutrality coefficients are presented. Table 3 below lists the design parameters of these extreme merit values. Since the length is the key design factor for solid propellant motors, the grain length is takes as the primary entry in the table below. The corresponding value of the other merit is also shown.

For all grain lengths, cylindrical designs yield the maximum filling coefficient. For short and medium-length grains, the maximum possible web thickness is ($\tau^* = 0.8$, for the used type of propellant). Grains with web thickness ($\tau^* = 0.9$) are not shown in the table since they all experience an erosive burning regardless to their length. As the grain length increases, erosive burning takes place in grains with ($\tau^* = 0.8$) and the maximum allowable grain thickness for such long grains is ($\tau^* = 0.7$) resulting in a drop in the filling coefficient. Grains with minimum filling are indeed the ones with minimum web thickness and taper angles of both ends regardless to the grain length. The filling coefficient increases slightly as the grain length increases. The values of neutrality corresponding to maximum and minimum filling are not the "desired" minimum nor the maximum ones, respectively. In contrast, no specific criteria can be identified for designs with the best (minimum) neutrality. However, the best neutrality can be related to small taper angles on both ends resulting in low filling. Of all samples tested, the grain lengths of 2, 4, and 4.5 the outer diameter yield the best neutrality. Grains as short as half the caliber yield the worst neutrality compared with longer grains.

Table 3: Grain designs with extreme neutrality and filling coefficients

L^*	Best (minimum) neutrality					Worst (maximum) Neutrality				
	N	τ^*	θ_h	θ_n	K_F	N	τ^*	θ_h	θ_n	K_F
0.5	1.6473	0.1	70	70	0.18	6.0174	0.1	10	10	0.12
1	1.1130	0.2	70	70	0.348	3.2303	0.3	10	10	0.29
1.5	1.0069	0.1	60	60	0.186	2.3173	0.5	10	10	0.42
2	1.0005	0.1	50	30	0.184	1.8398	0.6	10	10	0.51
2.5	1.0005	0.1	40	20	0.183	1.5642	0.7	10	10	0.58
3	1.0009	0.1	20	20	0.182	1.3344	0.6	10	10	1.33
3.5	1.0032	0.1	60	10	0.182	1.4271	0.8	60	70	0.92
4	1.0005	0.1	30	10	0.182	1.5214	0.7	60	60	0.87
4.5	1.0005	0.1	20	10	0.182	1.6637	0.7	60	60	0.88
5	1.0069	0.1	20	10	0.183	1.8108	0.7	60	60	0.88

L^*	Best (maximum) Filling					Worst (minimum) Filling				
	K_F	τ^*	θ_h	θ_n	N	K_F	τ^*	θ_h	θ_n	N
0.5	0.75	0.5	90	90	1.78	0.1224	0.1	10	10	6.017
1	0.96	0.8	90	90	1.23	0.1488	0.1	10	10	3.072
1.5	0.96	0.8	90	90	1.09	0.1603	0.1	10	10	2.113
2	0.96	0.8	90	90	1.09	0.1668	0.1	10	10	1.65
2.5	0.96	0.8	90	90	1.14	0.1710	0.1	10	10	1.39
3	0.96	0.8	90	90	1.26	0.1739	0.1	10	10	1.24
3.5	0.96	0.8	90	90	1.32	0.1760	0.1	10	10	1.14
4	0.91	0.7	90	90	1.38	0.1776	0.1	10	10	1.076
4.5	0.91	0.7	90	90	1.48	0.1789	0.1	10	10	1.036
5	0.91	0.7	90	90	1.6	0.1800	0.1	10	10	1.013

As inferred from Table 3 as well as from Fig. 5, no single grain can achieve both maximum filling and minimum neutrality. If a compromise design is sought, a new formula aggregating both merits is proposed. The proposed compromise merit function is defined here as the ratio between neutrality and filling, N/K_F; a grain design with a minimum value of N/K_F is considered better in both objectives and vice versa. The grain designs with extreme values of the proposed formula are listed in Table 4 with grain length as the main entries. The corresponding values for both N and K_F are listed. Generally, thick grains with right end(s) yield the minimum (best) values of the proposed merit function. In contrast, thin grains with highly-tapered ends yield the maximum (worst) merit function values. Of all grain designs tested, a 2-caliber long grain would yield the best merit function value. It should be noted that if a definition for the merit function other than the one proposed here, N/K_F, is adopted, the designs shown in Table 4 are expected to vary.

Table 4: Grain designs with extreme compromise merit function

L^*	Best (minimum) merit function; N/K_F					
	N/K_F	τ^*	θ_h	θ_n	N	K_F
0.5	2.3704	0.5	90	90	1.7778	0.75
1	1.2847	0.8	90	90	1.2333	0.96
1.5	1.1362	0.8	90	90	1.0907	0.96
2	1.1343	0.8	90	90	1.0889	0.96
2.5	1.1910	0.8	90	90	1.1433	0.96
3	1.2770	0.8	90	90	1.2259	0.96
3.5	1.3798	0.8	90	90	1.3246	0.96
4	1.3610	0.7	10	90	1.0365	0.762
4.5	1.3568	0.7	10	90	1.0517	0.775
5	1.3741	0.7	10	90	1.0805	0.786

L^*	Worst (maximum) merit function; N/K_F					
	N/K_F	τ^*	θ_h	θ_n	N	K_F
0.5	49.143	0.1	10	10	6.0174	0.1224
1	20.6487	0.1	10	10	3.0717	0.1488
1.5	13.1785	0.1	10	10	2.1128	0.1603
2	9.9165	0.1	10	10	1.6543	0.1668
2.5	8.16739	0.1	10	10	1.3965	0.1710
3	7.1271	0.1	10	10	1.2393	0.1739
3.5	6.4743	0.1	10	10	1.1395	0.1760
4	6.9033	0.1	50	50	1.2983	0.1881
4.5	7.4138	0.1	50	50	1.3958	0.1883
5	7.9461	0.1	50	50	1.4974	0.1884

Conclusions

The ballistic behavior of internal-end burning solid propellant grains is inspected in the present work. Neutrality, filling and likelihood of erosive burning of such grain design have been collectively investigated through a parametric study involving four design parameters. It is found that, erosive burning can take place for thick and long grains. Neutrality and filling of normally (non-erosive) burning grains are found competing. Neutrality can be maximized using a grain with aspect ratios of 2: 2.5, web thickness of 0.1 and front and rear taper angles 50º, and 30º, respectively. On the other hand, filling can be maximized using a grain with aspect ratios of 1: 3.5 and a web thickness of 0.8 with no taper at both ends. The impact of the design parameters on the performance merits is explained and visualized. Recommendations for compromise grain designs are proposed.

A compromised grain can have aspect ratio and web thickness of 2 and 0.8, respectively, with no taper at both ends.

References

[1] Sutton, G. P., "Rocket Propulsion element," Seventh edition, John Wiley,1992.

[2] Barrere, M., Jaumotte, A., De veubeke, B. F. and Vandenkerckhove, J.," Rocket Propulsion," Elsevier publishing company, 1960.

[3] Noaman, H. R., Ahmed, M. Y., Abdalla, H. M. and Al-Sanabawy, M. A., "Neutrality of Taper-Ended Tubular Grains," 15th International Conference on Aerospace Sciences and Aviation Technology, ASAT – 15, May 28 - 30, 2013.

[4] A. Kamran, L. Guozhu, A. F. Rafique, S. Naz, and Q. Zeeshan, "Star Grain Optimization using Genetic Algorithm," in 51st AIAA/ASME/ASCE/AHS/ASC Structures, Structural Dynamics, and Materials Conference 18th AIAA/ASME/AHS Adaptive Structures Conference 12th, 2010, p. 3084.

[5] W. T. Brooks, "Ballistic optimization of the star grain configuration," Journal of spacecraft and rockets, vol. 19, pp. 54-59, 1980.

[6] S. Krishnan, "Design of Neutral Burning Star Grains," Journal of Spacecraft and Rockets, 1975, Vol. 12, No. 1, pp. 60-72.

[7] K. Albarado, R. Hartfield, W. Hurston, and R. Jenkins, "Solid Rocket Motor Design Using Hybrid Optimization" International Journal of Aerospace Engineering, Volume 2012, Article ID 987402.

[8] K. Nisar, L. Guozhu, and Q. Zeeshan, "A hybrid Optimization Approach for SRM Finocyl Grain Design," Chinese Journal of Aeronautics, Vol. 21, pp. 481-487, 2008.

[9] A. Kamran and L. Guozhu, "Design and Optimization of 3D Radial Slot Grain Configuration," Chinese Journal of Aeronautics, Vol. 23, pp. 409-414, 2010.

[10] M. A. Raza and W. Liang, "Design and Optimization of 3D Wagon Wheel Grain for Dual Thrust Solid Rocket Motors," Propellants, Explosives, Pyrotechnics, vol. 38, pp. 67-74, 2013.

[11] M. A. Raza and W. Liang, "Robust performance optimization of dual thrust rocket motor," Aircraft Engineering and Aerospace Technology, vol. 84, pp. 244-251, 2012.

[12] M. A. Raza and W. Liang, "Robust Design Optimization of 3D Tandem Grain Configuration for Dual Thrust Solid Rocket Motor," Proceedings of the 2010 NDIA Conference.

[13] W. R. Kirchner, Tapered Tubular Propellant Grain, U.S. Patent No. 3000317, Sept. 19, 1961

[14] Himanshu Shekhar, Design of Funnel Port Tubular Propellant Grain for Neutral Burning Profile in Rockets, Defence Science Journal, Vol. 59, No. 5, September 2009, pp. 494-498